

HYBRID LES-RANS: ESTIMATING RESOLUTION REQUIREMENTS USING TWO-POINT CORRELATIONS AND SPECTRA

Lars Davidson

Division of Fluid Dynamics, Department of Applied Mechanics
 Chalmers University of Technology, SE-412 96 Göteborg, Sweden
 web: www.tfd.chalmers.se/~lada

1 Introduction

In the present study, hybrid LES-RANS is used to simulate fully developed channel flow. Four different resolutions are used. The resolutions are analyzed using two-point correlations (streamwise and spanwise directions), the corresponding spectra, the spectra of the SGS dissipation and by presenting the wave number at which the maximum spectral SGS dissipation takes place. The issue of overly large resolved kinetic energies on coarse grids is discussed.

2 Numerical details

2.1 The Momentum Equations

The Navier-Stokes equations with an added turbulent/SGS viscosity read

$$\begin{aligned} \frac{\partial \bar{u}_i}{\partial t} + \frac{\partial}{\partial x_j} (\bar{u}_i \bar{u}_j) &= \delta_{1i} - \frac{1}{\rho} \frac{\partial \bar{p}}{\partial x_i} + \frac{\partial}{\partial x_j} \left[(\nu + \nu_T) \frac{\partial \bar{u}_i}{\partial x_j} \right] \\ \frac{\partial \bar{u}_i}{\partial x_i} &= 0 \end{aligned} \quad (1)$$

where $\nu_T = \nu_t$ (ν_t denotes the turbulent RANS viscosity) close to the wall for $y \leq y_{ml}$, otherwise $\nu_T = \nu_{sgs}$. The turbulent viscosity, ν_T , is computed from an algebraic turbulent length scale, see Table 1, and a transport equation is solved for k_T , see below. The density is set to one in all simulations. A driving constant pressure gradient, δ_{1i} , is included in the streamwise momentum equation.

2.2 Hybrid LES-RANS

A one-equation model is employed in both the URANS region and the LES region and reads

$$\begin{aligned} \frac{\partial k_T}{\partial t} + \frac{\partial}{\partial x_j} (\bar{u}_j k_T) &= \frac{\partial}{\partial x_j} \left[(\nu + \nu_T) \frac{\partial k_T}{\partial x_j} \right] + P_{k_T} - C_\varepsilon \frac{k_T^{3/2}}{\ell} \\ P_{k_T} &= -\tau_{ij} \bar{s}_{ij}, \quad \tau_{ij} = -2\nu_T \bar{s}_{ij} \end{aligned}$$

	URANS region	LES region
ℓ	$2.5n[1 - \exp(-0.2k^{1/2}n/\nu)]$	$\ell = \Delta$
ν_T	$0.09 \cdot 2.5k^{1/2}n[1 - \exp(-0.014k^{1/2}n/\nu)]$	$0.07k^{1/2}\ell$
C_ε	1.0	1.05

Table 1: Turbulent viscosities and turbulent length scales in the URANS and LES regions. n denotes the distance to the nearest wall. $\Delta = (\delta V)^{1/3}$

Case	Δx	Δz	N_x	N_z
Baseline	0.1	0.05	64	64
$2\Delta x$	0.2	0.05	32	64
$2\Delta z$	0.1	0.1	64	32
$4\Delta x$	0.4	0.05	16	64

Table 2: Test cases.

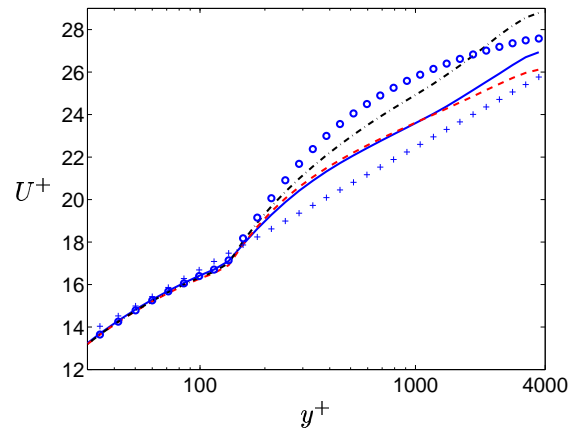


Figure 1: U velocities. — : Baseline; - - - : $2\Delta x$; ··· : $2\Delta z$; ○ : $4\Delta x$; + : $U^+ = (\ln y^+)/0.4 + 5.2$.

where $\nu_T = ck^{1/2}\ell$. The location at which the switch is made from URANS to LES is called the interface and is located at y_{ml} from each wall. In the inner region ($y \leq y_{ml}$) k_T corresponds to RANS turbulent kinetic energy, k ; in the outer region ($y > y_{ml}$) it corresponds to subgrid-scale kinetic turbulent energy, k_{sgs} . The coefficients are different in the two regions, see Table 1. No special treatment is applied in the equations at the matching plane except that the form of the turbulent viscosity and the turbulent length scale are different in the two regions. $k_T = 0$ at the walls. Greater detail is given in [1].

2.3 The Numerical Method

An incompressible, finite volume code is used [2]. For space discretization, central differencing is used for all terms except for the convection term in the k_T equation for which the hybrid central/upwind scheme is employed. The Crank-Nicolson scheme is used for time discretization of all equations. The numerical procedure is based on an implicit, fractional step technique with a multigrid pressure Poisson solver [3] and a non-staggered grid arrangement.

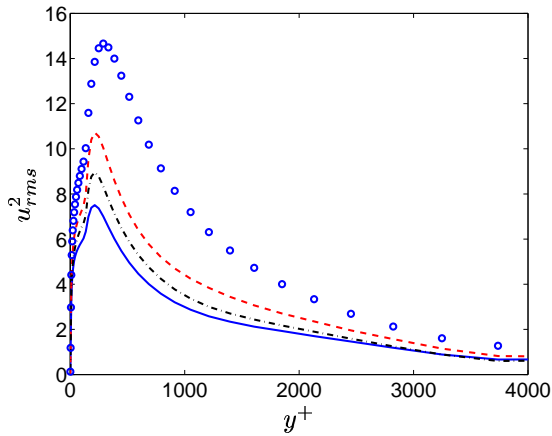


Figure 2: Resolved fluctuations in the streamwise direction. See caption in Fig. 1.

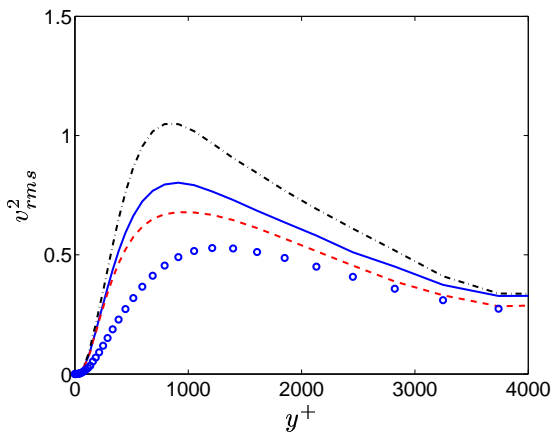


Figure 3: Resolved fluctuations in the wall-normal direction. See caption in Fig. 1.

3 Results

The flow was computed for Reynolds number $Re_\tau = u_\tau \delta / \nu = 4000$ (δ denotes the half width of the channel) and four different computational grids are used, see Table 2. The extent of the computational domain is $x_{max} = 6.2$ and $z_{max} = 3.2$ for all cases. The number of cells in the y direction is 80 with a constant geometric stretching of 15%. This gives a smallest and largest cell height of $\Delta y_{min}^+ = 2.2$ and $\Delta y_{max}^+ = 520$, respectively. The grid spacing in the wall-parallel plane in viscous units is $(\Delta x^+, \Delta z^+) = (400-1600, 200-400)$. The matching line is chosen along a fixed grid line at $y^+ = 125$ ($y = 0.0313$) so that 16 cells are located in the URANS region at each wall.

The velocity profiles are presented in Fig. 1. It can be seen that the Baseline case and Case $2\Delta x$ give almost the same results, whereas coarse spanwise spacing (Case $2\Delta z$) gives much poorer results. The coarsest streamwise grid spacing ($4\Delta x$) also yields poor agreement.

Figures 2 and 3 present the resolved fluctuations in the streamwise and wall-normal direction. As can be seen, u_{rms}^2 increases as the grid is coarsened, while v_{rms}^2 decreases as the grid is coarsened in the streamwise direction and increases upon coarsening in the spanwise direction; however, their product increases in all cases compared to the Baseline case. This can be explained as follows. The driving force term in the streamwise momentum equation must be balanced by the sum of the resolved, viscous and modelled shear stress. When

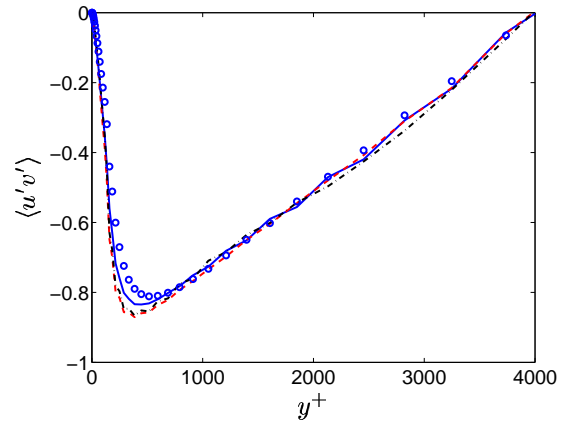


Figure 4: Resolved shear stress. See caption in Fig. 1.

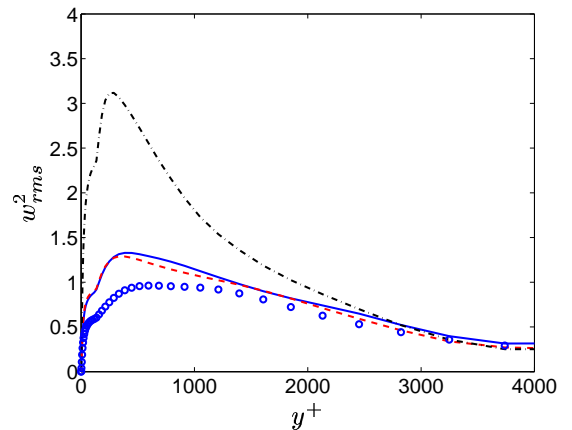


Figure 5: Resolved fluctuations in the spanwise direction. See caption in Fig. 1.

integrating the streamwise momentum equation, Eq. 1, in x , z , and t , we get

$$0 = y - \underbrace{\langle u'v' \rangle}_\tau \Big|_y + \underbrace{\left\langle (\nu + \nu_T) \frac{\partial \bar{u}}{\partial y} \right\rangle}_\tau \Big|_y - 1 \quad (2)$$

where the terms represent the prescribed driving pressure gradient, the resolved turbulent shear stress at y , the viscous and modelled turbulent shear stress at y , and the wall shear stress, respectively. We obtain the usual result: the total stress must behave as

$$\tau_{tot} = 1 - y \quad (3)$$

When the grid is coarsened, the non-linear interaction is weakened so that the correlation between the streamwise and wall-normal resolved fluctuations is diminished. This results in too small a resolved shear stress. The equations respond by increasing the resolved fluctuations by increasing the bulk velocity and hence the velocity gradient, $\partial \bar{u} / \partial y$, which is the main agent for producing resolved turbulence. The bulk velocity, and hence the resolved fluctuations, are increased until the resolved shear stress is large enough to satisfy Eq. 3. This phenomena also occurs for under-resolved DNS, see [1]. When the total turbulent (i.e. resolved plus modelled) kinetic energy is over-predicted in hybrid LES-RANS, as in the present simulations, it is often referred to as *double-counting*, meaning that the turbulent kinetic energy is accounted for twice, both by resolved

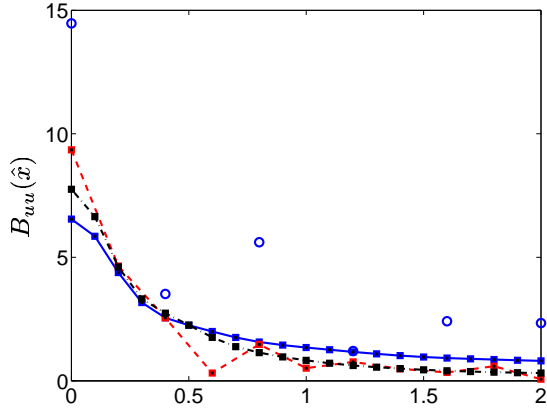


Figure 6: Two-point correlation $B_{uu}(\hat{x})$. $y = 0.083$. See caption in Fig. 1. Markers on the lines show the resolution.

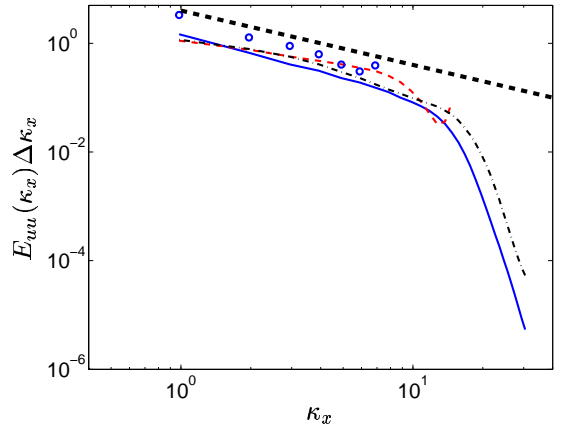


Figure 8: Energy spectrum $E_{uu}(\kappa_x)$. Thick dashed line shows $-3/3$ slope. $y = 0.083$. See caption in Fig. 1.

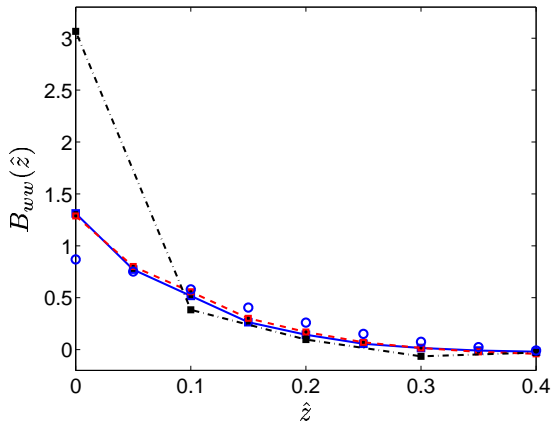


Figure 7: Two-point correlation $B_{ww}(\hat{z})$. See caption in Fig. 1. Markers on the lines show the resolution.

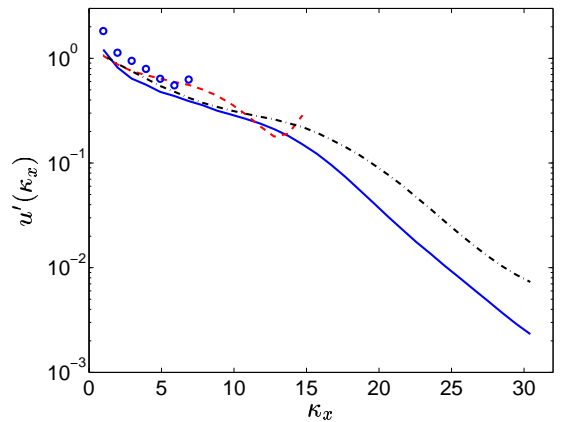


Figure 9: Spectrum of resolved streamwise fluctuations, $u' = (E_{uu}(\kappa_x)\Delta\kappa_x)^{1/2}$. $y = 0.083$. See caption in Fig. 1.

and modelled fluctuations. However, as explained above the reason is the prescribed driving pressure gradient in Eq. 1 along with the requirement in Eq. 3.

Figure 4 shows that the resolved shear stresses are essentially independent of grid resolution.

It should be stressed that the process of increasing the resolved fluctuations until the total shear stress satisfies Eq. 3 will not occur in a general flow case with an inlet and outlet (i.e. a flow case with no prescribed driving pressure gradient). In a general flow case, the resolved shear stresses will simply remain too small and the result will be underpredicted resolved shear stresses.

The spanwise resolved fluctuations are affected by grid coarsening in the same manner as the wall-normal ones: streamwise and spanwise coarsening cause a decrease and an increase, respectively, see Fig.5.

Figures 6 and 7 present the streamwise and spanwise two-point correlations, which are defined as $B_{uu}(\hat{x}) = \langle u'(x)u'(x - \hat{x}) \rangle_{xzt}$ and $B_{ww}(\hat{z}) = \langle w'(z)w'(z - \hat{z}) \rangle_{xzt}$, respectively (subscript xzt is added here to emphasize that two-point correlations are averaged over x , z and t). The two-point correlations are all presented for $y^+ \simeq 330$ ($y = 0.083$); the integration length scale decreases slightly closer to the wall and increases further away from the wall. Here we have chosen not to normalize the two-point correlations with u_{rms}^2 and w_{rms}^2 ,

respectively. When normalized, the comparison of the two-point correlations is very different, but the reason for the difference is primarily different levels of the resolved fluctuations. We can see from the two-point correlations that there are oscillations in $B_{uu}(\hat{x})$ for Cases $2\Delta x$ and $4\Delta x$. The two-point correlations also give an idea of how many grid cells are used to resolve the large scales. The large scales in the streamwise direction are resolved by 2 (Case $4\Delta x$) to 10 (Baseline case) cells whereas the large scales in the spanwise direction are covered by only 1 (Case $2\Delta z$) to 5 (Baseline case) cells. Thus, Figs. 6 and 7 indicate that all cases except the Baseline case have insufficient resolution.

Figure 8 presents the one-dimensional spectra $E_{uu}(\kappa_x)$. The thick dashed line shows the $-3/3$ slope. The spectra are computed by taking the Fourier transform of the two-point correlation, $B_{uu}(\hat{x})$, in Fig. 6. The spectra are all presented for $y^+ \simeq 330$ ($y = 0.083$) but, when plotted in log-log as in Fig. 6, they show the same behaviour across the channel, the main difference being that they are shifted along the E_{uu} axis as u_{rms}^2 varies across the channel. The smallest wavenumber is $\kappa_{x,min} = 2\pi/x_{max}$. The largest wavenumber included in the plots is $\kappa_{x,max} = 2\pi/2\Delta x$, where we have assumed that two cells are required to resolve a wavelength. For the Baseline case, for example, this gives

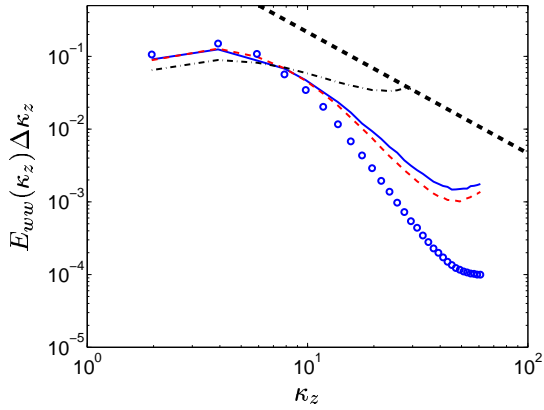


Figure 10: Energy spectra $E_{ww}(\kappa_z)$. The thick dashed line shows $-5/3$ slope. $y = 0.083$. See caption in Fig. 1.

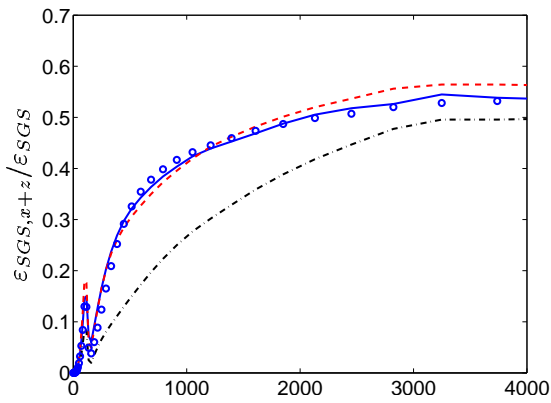


Figure 11: Ratio of SGS dissipation in the wall-parallel plane and in the y direction. $\epsilon_{SGS,x+z} = \epsilon_{SGS,11} + \epsilon_{SGS,33} + \epsilon_{SGS,13}$. See caption in Fig. 1.

$\kappa_{x,min} = 2\pi/6.4 = 0.98$ and $\kappa_{x,max} = \pi/0.1 = 31$. It can be seen in Fig. 8 that the spectra in all cases have a -1 slope, which indicates that the mesh resolution for these cases is too low. There is a pile-up of energy in the small streamwise scales for Cases $2\Delta x$ and $4\Delta x$. This phenomenon is present across the channel. In DNS and LES this phenomenon is usually attributed to too low a dissipation, which indicates too a low resolution. Here, it means that SGS dissipation

$$\epsilon_{SGS} = \langle \nu_T \frac{\partial \bar{u}_i}{\partial x_j} \frac{\partial \bar{u}_i}{\partial x_j} \rangle \quad (4)$$

is too small. This may be because the grid is too coarse or that the turbulent viscosity, ν_T , is too low. Note however that it is not necessarily the time-averaged SGS viscosity that is too low; the SGS dissipation may also be too small because the *correlation* between ν_T and $(\partial \bar{u}_i / \partial x_j)(\partial \bar{u}_i / \partial x_j)$ is too small. A SGS turbulence model with larger correlation between the instantaneous SGS viscosity and the small-scale resolved velocity gradients would perhaps work better in this case. Filtered SGS models [4] or variational multi-scale methods [5, 6, 7] might be an alternative since the SGS viscosity in these methods is computed using small-scale resolved fluctuations.

As noted above there are oscillations in the two-point correlation for Cases $2\Delta x$ and $4\Delta x$ (Fig. 6). If these

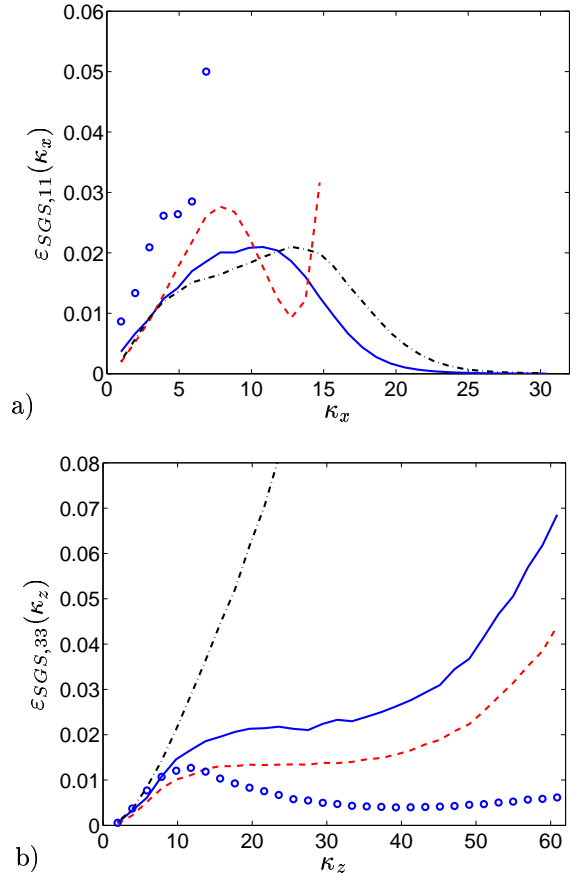


Figure 12: Spectra of approximated $\epsilon_{SGS,11}$ and $\epsilon_{SGS,33}$. $y = 0.083$. See caption in Fig. 1.

oscillations are smoothed out, the resulting spectra for Case $2\Delta x$ take a form similar to that of the spectra in Fig. 10. Hence the pile-up of energy in the small scales for Cases $2\Delta x$ and $4\Delta x$ is not a result of the oscillations in the two-point correlations.

For high wavenumbers ($\kappa_x > 10$), the streamwise spectra for the Baseline case and Case $2\Delta z$ exhibit a clear “dissipation” range (i.e. a steeper slope than $-5/3$). If the spectra had been obtained from DNS or experiments it would indeed have been a dissipation range, but in the present case we are using a turbulence model and hence what is seen in the spectra is a *SGS* dissipation range.

Apart from energy spectra $E_{uu}(\kappa_x)\Delta\kappa_x$, it is illustrative to plot the streamwise, resolved, spectral fluctuation, $u'(\kappa_x)$, see Fig. 9. Recall that (for details, see [8])

$$u_{rms}^2 = \sum_{k=1}^{nk} E_{uu}(k)\Delta\kappa_x \quad (5)$$

where $nk = 64$ (Baseline case) denotes number of cells in the spanwise direction and hence

$$u'(\kappa_x) = (E_{uu}(\kappa_x)\Delta\kappa_x)^{1/2}$$

The largest fluctuations in Fig. 9 can be compared with u_{rms} at $y^+ = 330$, which is equal to 3 for, for example, the Baseline case (see Fig. 2). Figure 2 shows that when the mesh is coarsened in the streamwise direction, the resolved fluctuations increase. Figures 8 and 9 show that it is the amplitudes of the fluctuations with the

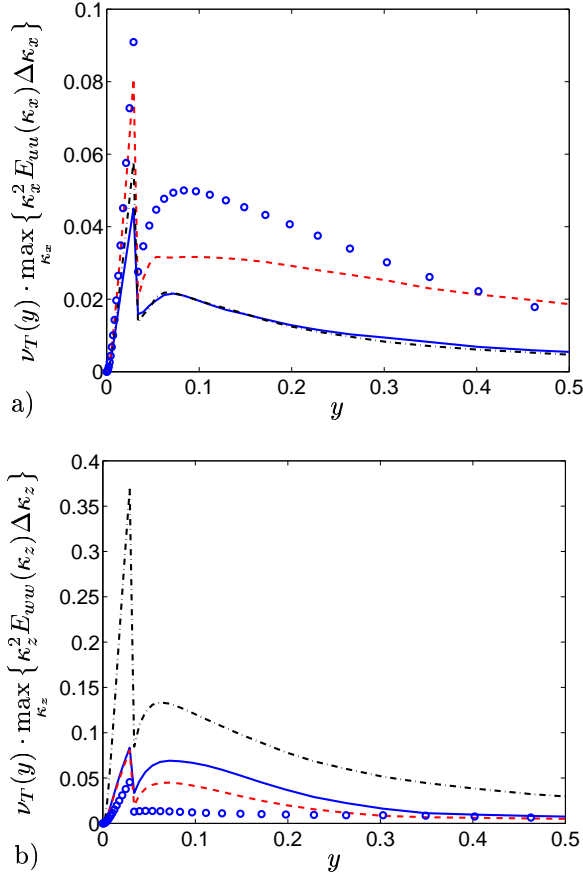


Figure 13: Maxima of modelled energy dissipation spectra. See caption in Fig. 1.

mid-range length scales ($1.8 < \kappa_x < 10$ or $2\pi/10 = 0.62 = 3.1\Delta x < \ell < 2\pi/1.8 = 3.5 = 17.5\Delta x$) that are enhanced for Case $2\Delta x$ when the mesh is coarsened in the streamwise direction, whereas the amplitudes are increased for all length scales for Case $4\Delta x$. Coarsening the grid in the spanwise direction (Case $2\Delta z$) results in a small increase in the amplitudes of the mid-range length scales and a larger increase in the intensity of the small scales ($\kappa_x > 10$).

Figure 10 shows the spanwise spectra of the spanwise fluctuations. Here we actually find some tendency of the spectra of the Baseline case and Case $2\Delta x$ to exhibit a $-5/3$ -slope. The spectra for all cases show a pile-up of energy in the small scales. This indicates that the spanwise resolution is too low.

The SGS dissipation, or the production of SGS turbulence, $P_{k,SGS}$, is given in Eq. 4. If we assume that

$$\varepsilon_{SGS,approx} \simeq \langle \nu_T \rangle \left\langle \frac{\partial \bar{u}_i}{\partial x_j} \frac{\partial \bar{u}_i}{\partial x_j} \right\rangle \quad (6)$$

we obtain the streamwise and spanwise components of the spectral SGS dissipation as [9]

$$\begin{aligned} \varepsilon(\kappa_x)_{11,SGS,approx} &\simeq \kappa_x^2 \langle 2\nu_T \rangle E_{uu}(\kappa_x) \Delta \kappa_x \\ \varepsilon(\kappa_z)_{33,SGS,approx} &\simeq \kappa_z^2 \langle 2\nu_T \rangle E_{ww}(\kappa_z) \Delta \kappa_z \end{aligned} \quad (7)$$

How important are these components of the SGS dissipation compared to the components involving the wall-normal direction, and especially that including $\partial \bar{u} / \partial y$? Figure 11 shows the ratio of the SGS dissipation in

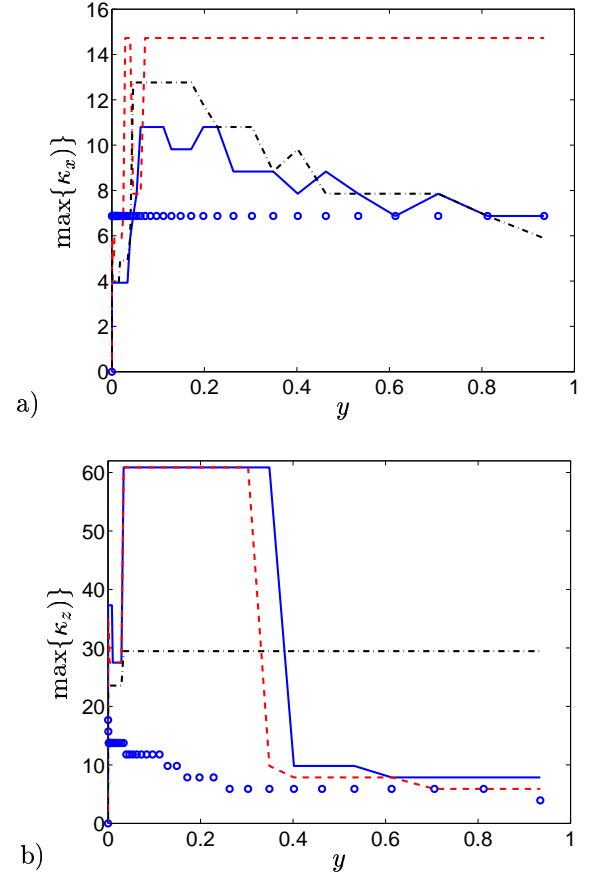


Figure 14: Wavenumber at which maxima in Fig. 13 occur. See caption in Fig. 1.

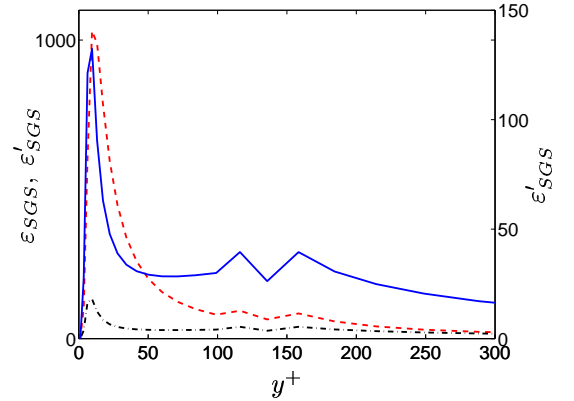


Figure 15: SGS dissipation. — : ε'_{SGS} (right scale); - - - : ε_{SGS} (left scale); - · - · : ε'_{SGS} (left scale).

the wall-parallel plane to the total SGS dissipation. At $y^+ \simeq 330$, for which location all the spectra above have been presented, the contribution of $\varepsilon_{SGS,x+z}$ to ε_{SGS} is close to 25% for all cases except Case $2\Delta z$. Thus it is relevant to look at the spectral content of $\varepsilon_{SGS,11}(\kappa_x)$ and $\varepsilon_{SGS,33}(\kappa_z)$ presented in Fig. 12. For the Baseline case, the peak of $\varepsilon_{SGS,11}(\kappa_x)$ is located at $\kappa_x \simeq 0.3\kappa_{x,max}$, see Fig. 12a. When the mesh is coarsened in the streamwise direction (Cases $2\Delta x$ and $4\Delta x$), the peak moves, as expected, to even lower wavenumbers. For Case $2\Delta x$ a peak also appears at the maximum wavenumber; it reflects the pile-up of energy at the highest wavenumbers in Fig. 10. The behavior of $\varepsilon_{SGS,33}(\kappa_z)$ in Fig. 12b for

the Baseline Case and Cases $2\Delta x$ and $2\Delta z$ shows that the SGS dissipation in the spanwise direction takes place in the smallest resolved scales. Both Cases exhibit a region ($10 < \kappa_z < 30$) where the SGS dissipation is constant. Cases $2\Delta z$ and $4\Delta x$ both exhibit a peculiar form of $\varepsilon_{SGS,33}(\kappa_z)$, indicating that the resolution and/or the SGS model is inappropriate; no region of constant SGS dissipation is found in the former case, but it increases monotonically up to 0.12 (not visible in Fig. 12b). In the latter case the peak of $\varepsilon_{SGS,33}(\kappa_z)$ occurs at $\kappa_z \simeq 10$.

Above we have presented the spectra at $y = 0.083$. Figure 13 shows the maximum spectral dissipation across the channel, and Fig. 14 presents the corresponding wavenumber. For example, the maximum spectral $\varepsilon_{SGS,11}(\kappa_x) \simeq 0.02$ at $y = 0.083$ occurs at $\kappa_x = 10$ (see Fig. 12a). This can also be seen in Fig. 13a; at $y = 0.083$ we see that $\nu_T(y) \cdot \max_{\kappa_z} \{ \kappa_z^2 E_{ww}(\kappa_z) \Delta \kappa_z \} \simeq 0.02$ and in Fig. 14a it can be seen that at $y = 0.083$, $\kappa_{x,max} \simeq 10$. Figure 13 shows that the maximum spectral SGS dissipation takes place in the URANS region, both for the streamwise and the spanwise components. In the LES region the spectral SGS dissipation decreases monotonically for increasing wall distance. Figure 14a shows that, for the Baseline case, the maximum SGS dissipation moves towards lower wavenumbers (larger scales) for increasing wall distance. In both Cases $2\Delta x$ and $4\Delta x$ the maximum SGS dissipation takes place at the highest wavenumbers (smallest resolved scales) across the channel.

Figure 14b presents the wavenumber at which the spanwise component of the spectral SGS dissipation attains its maximum. In the inner region ($y < 0.4$) the maximum SGS dissipation takes place at the highest wavenumbers for the Baseline case and Cases $2\Delta x$ and $2\Delta z$.

The spectra of the components of the SGS dissipation in Fig. 12 indicate that, when the grid is coarsened too much in one direction, this is exhibited as a monotonic increase of SGS spectral dissipation for increasing wavenumbers (without any region of constant SGS dissipation). This occurs for both Case $4\Delta x$ and Case $2\Delta z$. It seems that, for the streamwise component, this is close to taking place for Case $2\Delta x$ as well (double peak in Fig. 12a). Figure 14 shows that, when it occurs, it takes place across almost the entire channel.

Figure 15 presents the SGS dissipation, ε_{SGS} , see Eq. 4. As can be seen, it increases strongly near the wall in the URANS region, where it attains values 1000 times larger than those in the LES region. Figure 12 shows the streamwise and spanwise spectral components of the SGS dissipation. The SGS dissipation in Fig. 12 is due to the instantaneous *total* strain rates, $\partial \bar{u}_i / \partial x_j$. In Fig. 15 the SGS dissipation due to the fluctuating resolved strain rates

$$\varepsilon'_{SGS} = \varepsilon_{SGS} - \langle \nu_T \rangle \left(\frac{\partial \langle \bar{u} \rangle}{\partial y} \right)^2 \quad (8)$$

is also included. As can be seen, ε'_{SGS} and ε_{SGS} do not differ a great deal for $y^+ > 200$. However, in the URANS region (i.e. for $y^+ < 125$), the difference is very large. As the wall is approached, ε_{SGS} increases rapidly because of an increasing $\partial \langle \bar{u} \rangle / \partial y$, whereas **the increase in ε'_{SGS} is much smaller**. If, as mentioned above, new hybrid models based on the variational multi-scale methods are to be developed, this fact must be kept in mind. The turbulence viscosity in the URANS region should

probably not be computed with test-filtered strain rates, $\partial \hat{u}'_i / \partial x_j$ ($\hat{u}'_i = \hat{u}_i - \bar{u}_i$ where $\hat{\cdot}$ denotes test filtering). Instead the instantaneous resolved strain rate, $\partial \bar{u}_i / \partial x_j$, should be used.

4 Conclusions

Four different grid resolutions have been investigated: Baseline ($\Delta x, \Delta z$), two cases with coarsened grid in the streamwise direction ($2\Delta x, \Delta z$ and $4\Delta x, \Delta z$) and one case with coarsened grid in the streamwise direction ($\Delta x, 2\Delta z$). It is found that poor streamwise resolution results in oscillating streamwise two-point correlation. Poor spanwise resolution yields almost zero two-point correlation at separation of one cell. The energy spectra of u_{rms}^2 exhibit a -1 slope for all cases. For Cases $2\Delta x$ and $4\Delta x$, there is a pile-up of energy at the smallest resolved scales. The energy spectra of w_{rms}^2 for the Baseline case and Case $2\Delta x$ exhibit a $-5/3$ range. The spectra of the components of the approximated SGS dissipation shows a reasonable form for the Baseline case and Case $2\Delta x$.

The conclusion of the summary above is that the resolution for the Baseline case and Case $2\Delta x$ seems to be reasonable when looking at all quantities except the energy spectra of u_{rms}^2 .

Acknowledgments

This work was financed by the **DESider** project (Detached Eddy Simulation for Industrial Aerodynamics) which is a collaboration between Alenia, ANSYS-AEA, Chalmers University, CNRS-Lille, Dassault, DLR, EADS Military Aircraft, EUROCOPTER Germany, EDF, FOI-FFA, IMFT, Imperial College London, NLR, NTS, NUMECA, ONERA, TU Berlin, and UMIST. The project is funded by the European Community represented by the CEC, Research Directorate-General, in the 6th Framework Programme, under Contract No. AST3-CT-2003-502842.

Bibliography

- [1] L. Davidson and M. Billson. Hybrid LES/RANS using synthesized turbulence for forcing at the interface. *International Journal of Heat and Fluid Flow*, 27(6):1028–1042, 2006.
- [2] L. Davidson and S.-H. Peng. Hybrid LES-RANS: A one-equation SGS model combined with a $k - \omega$ model for predicting recirculating flows. *Numerical Methods in Fluids*, 43:1003–1018, 2003.
- [3] P. Emvin. *The Full Multigrid Method Applied to Turbulent Flow in Ventilated Enclosures Using Structured and Unstructured Grids*. PhD thesis, Dept. of Thermo and Fluid Dynamics, Chalmers University of Technology, Göteborg, 1997.
- [4] P. Sagaut, P. Comte, and F. Ducros. Filtered subgrid-scale models. *Physics of Fluids A*, 12:233, 2001.
- [5] T.J.R. Hughes, A.A. Oberai, and L. Mazzei. Large eddy simulation of turbulent channel flows by the variational multiscale method. *Physics of Fluids A*, 13:1784–1799, 2001.
- [6] P. Sagaut and V. Lévassieur. Sensitivity of spectral variational multiscale methods for large-eddy simulation of isotopic turbulence. *Physics of Fluids A*, 17(035113), 2001.
- [7] A.W. Vreman. The filtering analog of the variational multiscale method in large-eddy simulation. *Physics of Fluids A*, 15:L61–L64, 2003.
- [8] L. Davidson. How to make energy spectra with Matlab (available at www.tfd.chalmers/~lada). Report 2006/05, Div. of Fluid Dynamics, Dept. of Applied Mechanics, Chalmers University of Technology, Göteborg, Sweden, 2006.
- [9] J.O. Hinze. *Turbulence*. McGraw-Hill, New York, second edition, 1975.